COMPUTER METHODS IN APPLIED MECHANICS AND ENGINEERING 66 (1988) 45–63
NORTH-HOLLAND

A FINITE ELEMENT COMPUTATION OF TURBULENT BOUNDARY LAYER FLOWS WITH AN ALGEBRAIC STRESS TURBULENCE MODEL

Sang-Wook KIM and Yen-Sen CHEN
Fluid Dynamics Branch, ED 42, Systems Dynamics Laboratory, NASA/MSFC, Huntsville, AL 35812, U.S.A.

Received 14 October 1986
Revised manuscript received 11 February 1987; 8 July 1987

A finite element computational procedure for turbulent boundary layer flows and an algebraic stress turbulence model are presented. The finite element method is based on the semi-discrete Galerkin finite element method, the convergence nature of which has been reported previously. The algebraic stress turbulence model used in the present study can be characterized by the following three aspects: firstly, the eddy viscosity expression was derived from the Reynolds stress turbulence model; secondly, the turbulent kinetic energy dissipation rate equation was improved by including a production range time scale; and lastly, the diffusion coefficients for turbulence equations were adjusted so that the kinetic energy profile extends further into the free stream region which can be found in most of experimental data. Example problems considered include: a fully developed channel flow, a fully developed pipe flow, a flat plate boundary layer flow, a plane jet exhausting into a moving stream, a circular jet exhausting into a moving stream, and a wall jet flow. Computational results compared favorably with experimental data for most of the example problems considered. Significantly improved computational results were obtained for the plane jet flow and the wall jet flow, whereas rest of the computational results were comparable to those obtained by finite difference methods using the standard k-ε turbulence model.

1. Introduction

During the last decades, significant progress has been made in mathematically modelling the turbulent flows. Memorable events in the effort, among many others, would be the two Stanford conferences on turbulent flows [1, 2].

Development of turbulence models, and accordingly computation of turbulent flows too, were made, entirely to certain extents, using one or another form of the finite difference method. In the course of development using the finite difference method, turbulent boundary layer flows have been solved more frequently than elliptic flows. This can be attributed to its importance in engineering applications and, more importantly, to the simplicity of the boundary layer equations and abundant number of experimental data for different flow situations that can be used advantageously for verification of turbulence models.

Only very recently, a few publications on finite element computation of turbulent flows began to appear. Among these are [3–9].

A few difficulties observed in these finite element computations of turbulent flows are summarized below. In any turbulent flow, parabolic or elliptic, the turbulence dissipation rate and the production rate varies a few orders of magnitude in extremely small spatial distance. Consequently, a slight disturbance which may occur during the iterative solution procedure may render the system of equations hard to converge. Thomas et al. [6] presented an iteration procedure dedicated to overcome this difficulty. Hutton and Smith [8] expressed difficulty in preparing initial guess to obtain convergent solutions. Smith [3] also reported that the turbulent kinetic energy and/or the dissipation rate (ε) may become negative during iterations so that these negative numbers were set to be positive to obtain convergent solution. In the present paper, a strongly convergent relaxation technique [10], which is more or less a standard procedure in the finite difference methods, was used to overcome this difficulty.

It was also reported in some of these literatures that finite element computation of turbulent flows using the standard k-ε turbulence model yielded poor computational results. For example, Smith [3] reported that the standard k-ε turbulence model yielded a kinetic energy profile with strong peak near the backward-facing step, but such peak was not found in experimental data for the same flow. Taylor et al. [4] reported that an unacceptably bad computational result was obtained for a backward-facing step flow, i.e., the reattachment length was by far too short compared with experimental data. The turbulence model presented in this paper significantly improved the computational results as can be found in the later sections.

Unlike the finite difference computation of turbulent flows, there exists a further limited number of finite element computation of boundary layer flows. Among these are Taylor et al. [5] and Soliman and Baker [9]. In Taylor et al. [5] an elliptic flow solver was used to solve boundary layer flows using a k-ε turbulence model. In Soliman and Baker [9] linear Lagrangian elements were used to discretize the domain in normal to the flow direction, and nonorthogonal grid transformation was used to achieve computational efficiency. The finite element method proposed by Soliman and Baker [9, 11] showed convergence nature which is in good agreement with the theory of finite elements [12] for the linear element case, which has been used in their turbulent boundary layer flow calculation. The finite element computational procedure for laminar boundary layer flows proposed in Kim and Payne [13] exhibited convergence nature which is consistent with the theory of finite elements for all the types of elements considered, i.e., the linear element, the quadratic element, and the Hermite cubic element. It was also shown in a previous study [13] that the linear element was inferior to the quadratic element; hence, only the quadratic element is considered in the present study. It can be concluded that the finite element computation of turbulent boundary layer flows is not as exhaustive as the finite difference computation of the same class of flows.

Considering the success of the finite element method in other areas of engineering computations, such as structural mechanics, laminar flow problems, and chemical process modelling to mention a few, it is quite unusual that the finite element method has been hardly used for computation of turbulent flows especially when k-ε type turbulence models are used.

A finite element turbulent boundary layer flow analysis code, which is based on the finite element laminar boundary layer flow analysis code, has been constructed to assess and/or validate turbulence models to be used for general finite element computation of turbulent flows. The numerical details on turbulence equations are described in later sections, whereas all the numerical details on boundary layer flow equations can be found in [13].

Use of the present turbulence model in finite difference computation of turbulent boundary layer flows as well as elliptic flows improved the computational results in comparison with those obtained by using the standard k-ε turbulence model [14].

2. Turbulent flow equations

The standard turbulent boundary layer equations are given as:

$$\frac{\partial u}{\partial x} + \frac{1}{y^r}\frac{\partial}{\partial y}(y^r v) = 0, \tag{1}$$

$$u\frac{\partial u}{\partial x} + v\frac{\partial u}{\partial y} - \frac{1}{y^r}\frac{\partial}{\partial y}\left\{(\nu + \nu_t)y^r\frac{\partial u}{\partial y}\right\} = -\frac{\mathrm{d}p}{\mathrm{d}x}, \tag{2}$$

where u and v are time averaged velocities in the flow direction and in the transverse direction, respectively, p is the pressure, ν is the kinematic viscosity of the fluid, ν_t is the turbulent eddy viscosity, and r is an integer such that $r = 0$ for two-dimensional flows and $r = 1$ for axisymmetric flows.

3. Turbulence model

3.1. Eddy viscosity equation

The eddy viscosity expression can be obtained by contracting the Reynolds stress turbulence model [15] using an algebraic Reynolds stress transport assumption [16]. In most of the algebraic stress turbulence models, the eddy viscosity is given as [16, 17];

$$\nu_t = c_\mu k^2/\varepsilon, \tag{3}$$

$$c_\mu = \frac{2}{3}\frac{(1 - c_{v2})(c_{v1} - 1 + c_{v2}P/\varepsilon)}{(c_{v1} - 1 + P/\varepsilon)^2}, \tag{4}$$

where ν_t is the turbulent eddy viscosity; k is the turbulent kinetic energy; ε is the dissipation rate; P, $P = \nu_t(\partial u/\partial y)^2$, is the production rate; u is the time averaged flow direction velocity; y is the transverse coordinate; $c_{v1} = 3.7 + 0.7\tanh(P/\varepsilon)$; and $c_{v2} = 0.32$.

The functional form of c_{v1} was used to bring down c_μ to 0.09 for equilibrium state (the production rate is equal to the dissipation rate of turbulent kinetic energy). The c_μ curve is shown in Fig. 1 together with that of Launder [17]. A different c_μ curve can also be found in [16]. Experimentally deduced c_μ curves [16] are also shown in Fig. 1. Detailed discussions on the c_μ function can be found in [16, 17].

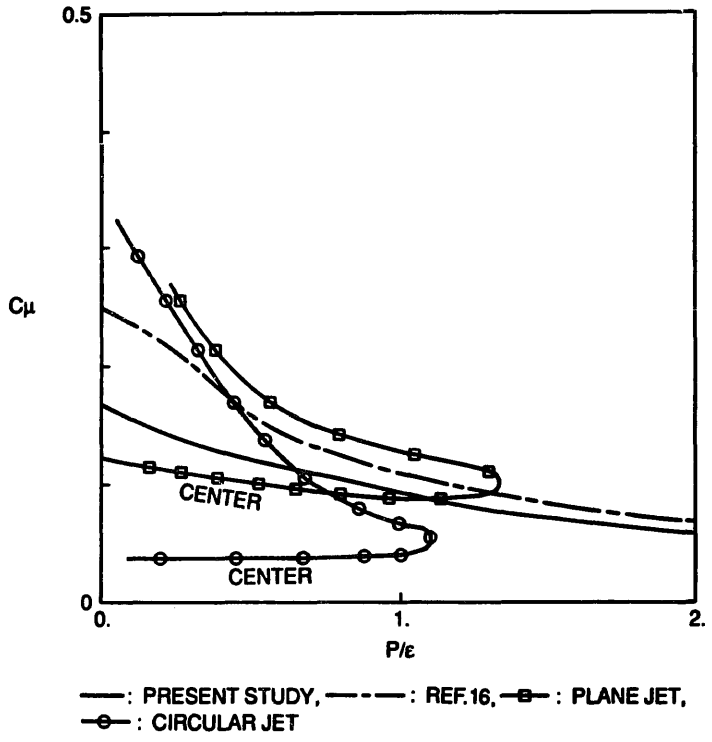

Fig. 1. Function C_μ.

3.2. Turbulence equations

The transport equation for turbulent kinetic energy is given as:

$$\frac{Dk}{Dt} = P - \varepsilon + \frac{1}{y^r}\frac{\partial}{\partial y}\left\{y^r\left(\nu + \frac{\nu_t}{\sigma_k}\right)\frac{\partial k}{\partial y}\right\}. \tag{5}$$

Many of the experimental data, such as the flat plate boundary layer flow due to Klebanoff [18] and turbulent jets exhausting into moving streams [19, 20] considered herein as example problems, show that the turbulent kinetic energy and its gradient are persistently big even after the velocity gradient has vanished near and in the free stream region. It is argued that the turbulent kinetic energy has been diffused outward from the high turbulence region due to the following reasons. Firstly, the velocity gradient has vanished and there is no production of turbulent kinetic energy in the region. Secondly, the boundary layer flows are spreading in the down-stream direction, hence the turbulent kinetic energy couldn't have been convected from the up-stream region. Thirdly, the decay rate of turbulence, as can be found in the grid turbulence, is so small that the same level of turbulent kinetic energy should exist throughout the free stream region if it has been convected from the high turbulence region. Consequently, the diffusivity of turbulent kinetic energy has to be bigger than that of the momentum equation, and hence the diffusion coefficient, σ_k, for turbulent kinetic energy has to be smaller than unity to achieve the observed diffusion process of the turbulent kinetic energy.

It has long been recognized that the standard dissipation rate equation has a lack of variable energy transfer capability which will transfer more turbulent kinetic energy into the dissipation

range when production is high. The same line of efforts to introduce a variable energy transfer function into the standard dissipation rate equation can be found in papers by Pope [21], Hanjalic and Launder [22], and Hanjalic et al. [23], among many others.

In [24] it was proposed to let part of the dissipation rate (ε) evolve according to a time-scale related to the production itself. The proposed dissipation rate equation is given as:

$$\frac{D\varepsilon}{Dt} = \frac{\varepsilon}{k}(c_1'P - c_2'\varepsilon) + \frac{P}{k}(c_3'P - c_4'\varepsilon) + \frac{1}{y^r}\frac{\partial}{\partial y}\left\{y^r\left(\nu + \frac{\nu_t}{\sigma_\varepsilon}\right)\frac{\partial \varepsilon}{\partial y}\right\}, \tag{6}$$

where D/Dt represents material derivative; σ_ε is a constant; and the rest of the notations is the same as before. In (6), k/ε can be considered to be a time scale related to the dissipation rate, and k/P to the production rate. After simplification, (6) becomes:

$$\frac{D\varepsilon}{Dt} = c_1\frac{P\varepsilon}{k} - c_2\frac{\varepsilon^2}{k} + c_3\frac{P^2}{k} + \frac{1}{y^r}\frac{\partial}{\partial y}\left\{y^r\left(\nu + \frac{\nu_t}{\sigma_\varepsilon}\right)\frac{\partial \varepsilon}{\partial y}\right\}. \tag{7}$$

The model constants used in the present study are: $\sigma_k = 0.75$, $\sigma_\varepsilon = 1.05$, $c_1 = 1.15$, $c_2 = 1.90$, and $c_3 = 0.25$.

The present proposition that $\sigma_k = 0.75$ coincides with the statements that $\sigma_k = 0.74$ improved the computational results as can be found in [25]. Further discussions on these two coefficients can be found in [26].

3.3. *Wall function boundary conditions*

The standard wall function boundary conditions were used in the present study. These are given as:

$$\frac{u}{u_\tau} = \frac{1}{\kappa}\ln(Ey^+), \tag{8}$$

$$k = c_\mu^{-1/2}\tau_w/\rho, \tag{9}$$

$$\varepsilon = c_\mu^{3/4}k^{3/2}/\kappa y, \tag{10}$$

where u^+, $u^+ = u/u_\tau$, is a nondimensional velocity; u_τ, $u_\tau = \sqrt{\tau_w/\rho}$, is the wall friction velocity; τ_w is the wall shearing stress; y^+, $y^+ = u_\tau y/\nu$, is the wall coordinate; κ is the von Karmann constant; and E is an experimentally determined constant coefficient. The most frequently used values of κ and E, i.e. $\kappa = 0.4$ and $E = 9.0$, were used in the present study. The wall function boundary conditions are more appropriate for the wall coordinate, y^+, greater than 80 and probably less than 300, as can be found in [27].

In the standard wall function methods, it is implicitly implied that the production rate is equal to the dissipation rate of turbulent kinetic energy, hence $c_\mu = 0.09$ at the near wall region as can be confirmed in (4). After some algebra, (8) can be rewritten as:

$$\tau_w = -\{\rho\kappa c_\mu^{1/4}k^{1/2}/\ln(Ey^+)\}u. \tag{11}$$

The boundary layer flows considered in the present study can be divided into two groups for convenience in discussions. These are: elliptic boundary layer flows such as the fully developed channel flow for which initial condition data are not required; and parabolic boundary layer flows such as the wall jet flow for which both initial and boundary conditions need to be prescribed to complete the problem definition.

The validity of standard wall functions has been questioned by many turbulence investigators including Chen [28]. A vast number of publications on the topic can be found in [28]. It would be enough to cite here that the wall function boundary conditions are approximately true. Therefore, Dirichlet boundary conditions as obtained directly from the experimental data were used for the near wall boundary conditions of elliptic boundary layer flows. For parabolic boundary layer flows, a Neumann (flux) boundary condition as given in (10) was used for the momentum equation and the Dirichlet boundary conditions as given in (8) and (9) were used as the near wall boundary conditions for the turbulence equations.

A vanishing gradient boundary condition was used at the outer edge of the computational domain for all the cases. This boundary condition is mathematically clean [29] and does not introduce any approximation error for boundary conditions at the outer edge of the flow domain.

4. Finite element computational procedure

Details of the present finite element computational procedure for turbulent boundary layer flows are described below. Convergence study of the numerical method used can be found in [13].

The transverse computational domain was extended outward several times the boundary layer thicknesses at the initial line of the flow direction computational domain, and orthogonal grids were used everywhere in the flow domain in order to avoid even the slightest source of numerical uncertainty [13] that can be caused by nonorthogonal grid transformation. This scheme was found to be especially helpful in assessing turbulence models to be used for multi-dimensional elliptic flow computations [14].

In order to enhance the numerical stability [10] the turbulence equations were rearranged as:

$$u\frac{\partial k}{\partial x}+v\frac{\partial k}{\partial y}-\frac{1}{y^r}\frac{\partial}{\partial y}\left\{y^r\left(\nu+\frac{\nu_t}{\sigma_k}\right)\frac{\partial k}{\partial y}\right\}+\left(\frac{\varepsilon}{k}\right)k=P\,, \tag{12}$$

$$u\frac{\partial \varepsilon}{\partial x}+v\frac{\partial \varepsilon}{\partial y}-\frac{1}{y^r}\frac{\partial}{\partial y}\left\{y^r\left(\nu+\frac{\nu_t}{\sigma_\varepsilon}\right)\frac{\partial \varepsilon}{\partial y}\right\}+\left(c_2\frac{\varepsilon}{k}\right)\varepsilon=c_1\frac{P\varepsilon}{k}+c_3\frac{P^2}{k}\,. \tag{13}$$

Contributions of the source terms, $(\varepsilon/k)k$ and $(c_2\varepsilon/k)\varepsilon$ in (12) and (13) respectively, to the finite element system of equations for an element are given as:

$$B_{ij}^k=\int_{\Omega_e}\frac{\varepsilon_1\varphi_1}{k_m\varphi_m}\varphi_i\varphi_j y^r\,\mathrm{d}y\,, \tag{14}$$

$$B_{ij}^{\varepsilon} = \int_{\Omega_e} \frac{\varepsilon_1 \varphi_1}{k_m \varphi_m} \varphi_i \varphi_j y^r \, dy \,, \tag{15}$$

where B_{ij}^{k} and B_{ij}^{ε} are the source matrices for the turbulent kinetic energy equation and the dissipation rate equation, respectively; φ_i denotes a finite element interpolating polynomial; k_1 and ε_1 denote nodal values of the turbulent kinetic energy and the dissipation rate, respectively; Ω_e denotes an element; and any repeated index represents summation over the index for the number of nodes in an element. The rest of the discrete system of equations was obtained in the same way as in the flow direction momentum equation [13].

The above procedure was found to be especially useful for computation of the fully developed channel flow (which is a special case of boundary layer flows as well as a special case of elliptic flows) such that extremely bad initial guess (e.g., flat profiles) for all of the variables could be used for a Picard-type iterative solution scheme. It was also necessary to freeze the eddy viscosity (ν_t) profile (i.e., use the same eddy viscosity profile) in each iteration for the fully developed channel and pipe flows to enhance numerical stability. But these procedures were not necessary for parabolic boundary layer flows, because the flow direction derivative terms enhance numerical stability and hence the governing equations as given in (1), (2), (5), and (7) could be solved directly using the semi-discrete Galerkin method. It was found in the present study that both of the computational strategies yielded the same results for parabolic boundary layer equations within the limit of computer round-off error.

The global finite element system of equations is obtained by assembling the element system of equations, and evaluation of the element system of equations is performed using the Gauss numerical quadrature [30]. In general, an N-point quadrature rule can integrate polynomials of degree $(2N-1)$ or less exactly. In the present study, it was found that at least the four-point Gauss quadrature rule was required for the diffusion term for the resulting system of equations to be independent of numerical quadrature.

The production term contains a velocity gradient, $\partial u/\partial y$, which is best approximated at the two Gauss points when quadratic Lagrangian interpolating polynomials are used in the finite element analysis. The load vectors containing the production rate in (12) and (13) were integrated using the two-point Gauss quadrature rule, and rest of the terms were integrated using the four-point Gauss quadrature rule. In computing the term c_μ (4), which contains the production rate, the velocity gradient ($\partial u/\partial y$) was evaluated at the two-Gauss point and then interpolated and/or extrapolated to other locations inside of an element whenever necessary, which is a well-established technique in the finite element computational method [31, 32]. The production rate changes a few orders of magnitude in a small spatial distance, especially near the wall region. Hence a very fine grid need to be used near the wall region. But the present method was proved to be not so sensitive to grids used, and consequently, no special care need to be taken for grid generation other than that the grids near the wall region were approximately one-tenth of the largest grids in the outer free stream region.

In each iteration, the turbulent flow equations (1), (2), (5), and (7) were solved in a segregated sequence using a Picard (direct) iteration method employing underrelaxation. The updated solution (a_j^*) was obtained as:

$$a_j^* = (1-\alpha) a_j^n + \alpha a_j^{n+1} \,, \tag{16}$$

where a stands for u, k, or ε; α is an underrelaxation number; the superscript n denotes the iteration level; and the subscript j denotes the nodal degree of freedom. $\alpha < 0.6$ was required for elliptic boundary layer flows; but $\alpha = 1$ (no underrelaxation) was used for parabolic boundary layer flows.

For all of the cases, the convergence criterion used was given as:

$$|(a_j^{n+1} - a_j^n)/a_j^{n+1}| < e\,, \quad j = 1, \ldots, N, \text{ no sum on } j\,, \tag{17}$$

where N denotes the total number of degrees of freedom; and $e = 1 \times 10^{-7}$ was used. It can be seen that the present convergence criterion is extremely more demanding than that of Taylor et al. [5] where $e = 5 \times 10^{-3}$ was used.

5. Computational results

In all of the following computations, the governing differential equations were solved on the physical domain using physical dimensions. Whenever necessary, the values of 1.225 kg/m^3 and 0.17854×10^{-4} kg/m-sec were used for density and molecular viscosity, respectively.

For parabolic boundary layer flows, initial condition data for velocity and turbulent kinetic energy were obtained from experimental data, whereas the turbulence dissipation rate (ε) was prepared using the Boussinesq eddy viscosity assumption, that is:

$$\varepsilon = \frac{1}{-\overline{u'v'}}\, c_{\mu f} k^2 \frac{\partial u}{\partial y}\,, \tag{18}$$

where the Reynolds stress, $-\overline{u'v'}$, and $\partial u/\partial y$ were also obtained from experimental data, and $c_{\mu f} = 0.09$ has been used in (18).

For all of the example cases, 45 unequally spaced quadratic elements were used to discretize the transverse domain, unless otherwise specified.

5.1. *Fully developed channel flow*

The experimental data for the fully developed channel flow used herein can be found in [33]. One half of the channel width of 0.0635 meters, centerline mean velocity of 7.07 m/s (the Reynolds number based on these two parameters is approximately 30,800), a pressure gradient of -1.405 kg-m/s^2-m^3, and a wall friction velocity, u_τ, of 0.270 m/s were used.

The computational domain which extends from $y = 0.005$ m near the wall, which corresponds to $y^+ = 100$, to $y = 0.0635$ m at the center of the channel was discretized using 20 equally spaced quadratic elements. Near $y^+ = 40$ and below, high Reynolds number turbulence models may not yield good predictions unless these are modified by including low turbulence Reynolds number effects.

The Dirichlet boundary conditions for u and k at the near wall region were obtained from experimental data, whereas the boundary condition for ε was obtained from the mixing length assumption given below:

$$l = c_{\mu f}^{1/4} l_{\mathrm{m}}\,, \qquad l_{\mathrm{m}} = \kappa y\,, \qquad \varepsilon = c_{\mu f} k^{3/2}/l\,, \tag{19}$$

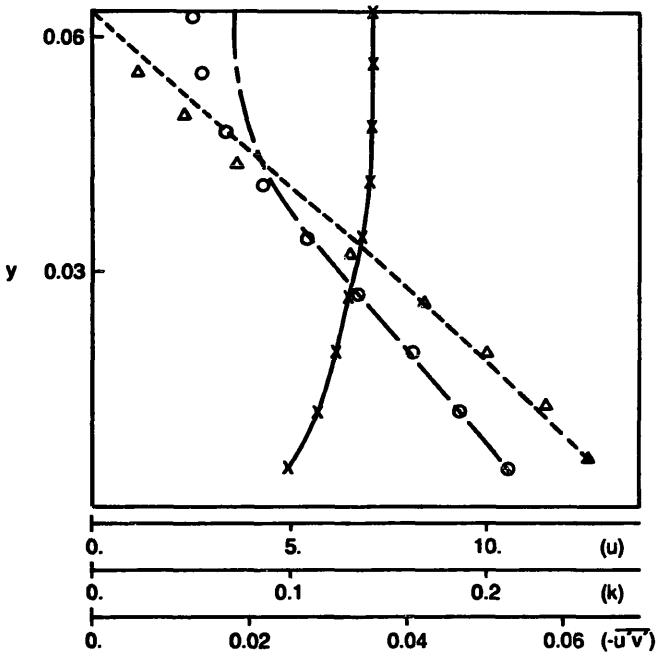

X: VELOCITY (u), O: KINETIC ENERGY (k), Δ: SHEARING STRESS ($-\overline{u'v'}$), ——, — — —, — — —: COMPUT. RESULT FOR u, k, and $-\overline{u'v'}$ RESPECTIVELY.

Fig. 2. Fully developed channel flow.

where l is the turbulence length scale and l_m is the mixing length. The near wall boundary conditions used are: $u = 5.084\,\text{m/s}$; $k = 0.213\,\text{m}^2/\text{s}^2$; and $\varepsilon = 10.64\,\text{m}^2/\text{s}^3$.

The convergence criterion stated earlier was achieved in 84 iterations. The computational results for the velocity, the turbulent kinetic energy, and the Reynolds stress are compared with the experimental data in Fig. 2. For the fully developed channel flow and the fully developed pipe flow, the flat profiles were used as initial guesses, and approximately 100 iterations were required to obtain the aforementioned convergence criterion. But in most of the parabolic boundary layer flows, the same convergence criterion was achieved in approximately 10 iterations, since the solution on the previous line-level, which is already close to the convergent solutions, was used as initial guesses.

It was found that the level of agreement between the present computational results and the experimental data was almost equivalent to that of finite difference computation of the fully developed channel flow using the standard k-ε turbulence model.

5.2. *Fully developed pipe flow*

The fully developed pipe flow is another case of elliptic boundary layer flow. The experimental data used can be found in [34]. The diameter of pipe is 0.24688 m, the center line velocity is 30.48 m/s, the Reynolds number based on these two parameters is 500,000, the pressure gradient in the flow direction is equal to $-23.05\,\text{kg-m/s}^2\text{-m}^3$, and the wall friction velocity is equal to 1.078 m/s.

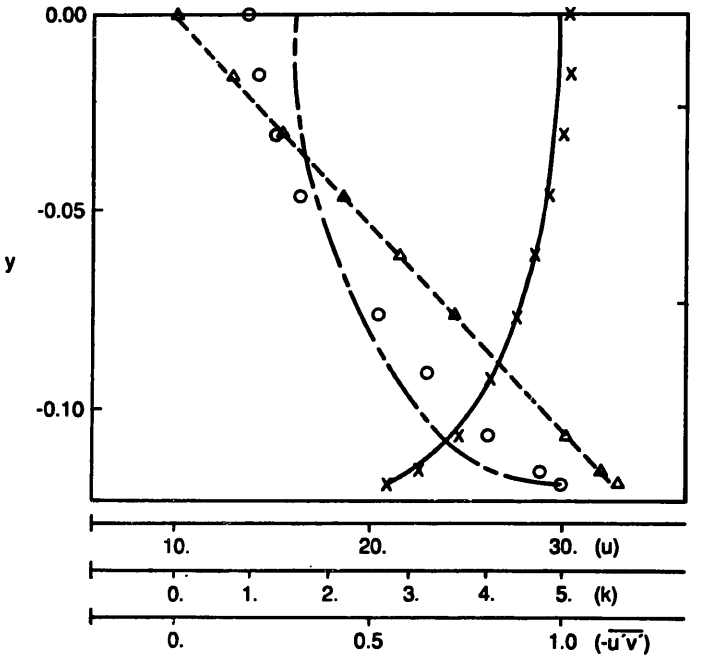

X: VELOCITY (u), O: KINETIC ENERGY (k), Δ: SHEARING STRESS ($-\overline{u'v'}$), ——, — — —, – – –: COMPUT. RESULT FOR u, k, and $-\overline{u'v'}$ RESPECTIVELY.

Fig. 3. Fully developed pipe flow.

The computational domain extending from $y = 0$ m at the center of the pipe to $y = 0.1192$ m at the near wall region, which corresponds to $y^+ = 300$, was discretized using 20 equally spaced quadratic elements. The near wall boundary conditions obtained from experimental data are given as: $u = 20$ m/s, $k = 4.93\,\text{m}^2/\text{s}^2$, and $\varepsilon = 1000\,\text{m}^2/\text{s}^3$. It took 100 iterations to achieve the same prescribed convergence criterion. The computational results are compared with experimental data in Fig. 3.

5.3. *Flat plate boundary layer flow under vanishing pressure gradient*

The Wiehardt and Tillmann flat plate boundary layer flow [35] is considered below. Another case of equilibrium boundary layer flow with zero pressure gradient can be found in [18]. Both of the flat plate boundary layer flows are self-similar flows. Experimental wall shearing stresses are presented by Wiehardt and Tillmann [35], whereas self-similar Reynolds stresses are given by Klebanoff [18]. In the following computation, the initial condition data for velocity were obtained from Wiehardt and Tillmann [35]; and the turbulent kinetic energy from Klebanoff [18].

The free stream velocity is equal to 33 m/s and the free stream turbulence level is 0.25 percent. The transverse computational domain extending from $y = 0.001$ m at the near wall region, which corresponds to $y^+ = 100$, to $y = 0.112$ m at the free stream region was discretized using 45 unequally spaced quadratic elements. The computational domain in the flow direction, which extends from $x = 9.937$ m up to $x = 4.987$ m was discretized using 600 line steps.

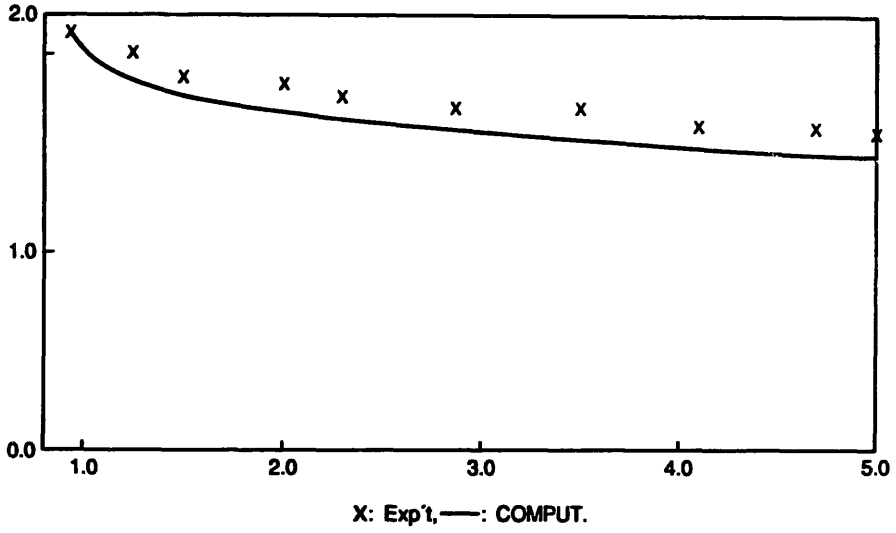

Fig. 4. Wall shearing stress for the flat plate flow.

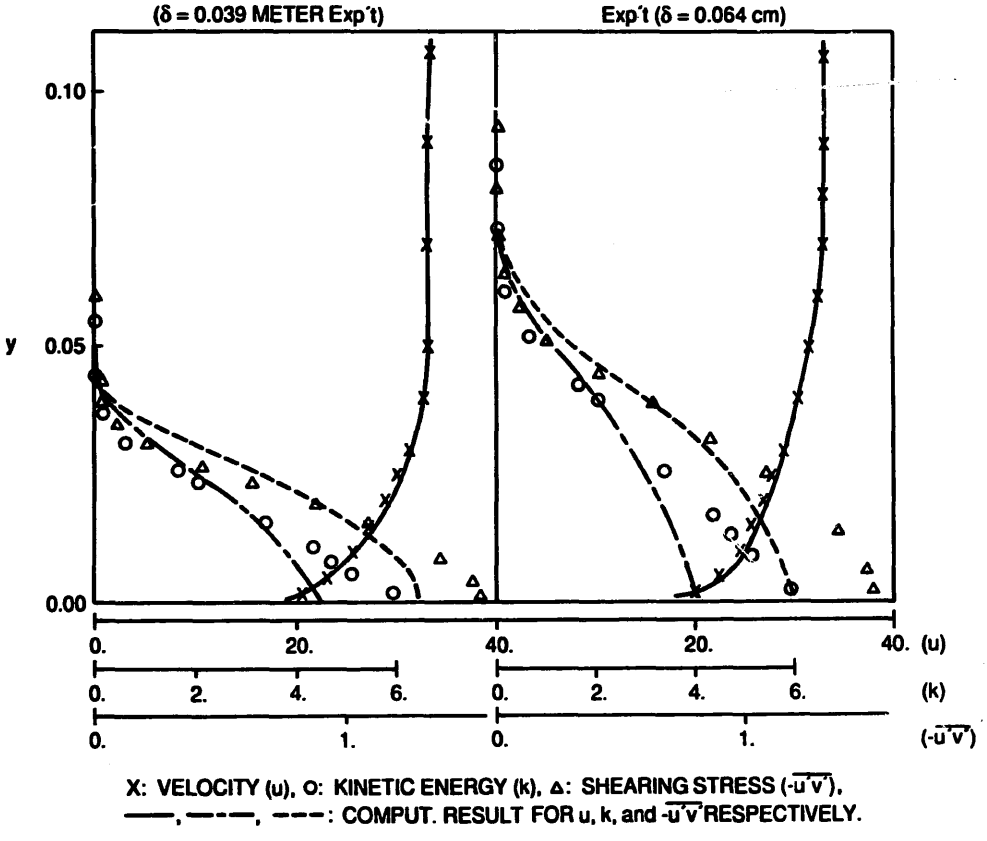

Fig. 5. Flat plate flow with zero pressure gradient.

Development of the wall shearing stress along the flow direction is shown in Fig. 4. The computed velocity profile, the kinetic energy profile, and the Reynolds stress are compared with experimental data in Fig. 5. Approximately 14 iterations were required for each line step. It can be seen in Fig. 5 that the velocity profile compares more favorably with experimental data than the turbulent kinetic energy and the Reynolds stress profiles. This may be due to the inconsistent initial condition data for the turbulent kinetic energy, which was obtained from another set of experimental data [18].

5.4. *A plane jet exhausting into a moving stream*

A plane jet exhausting into a moving stream is considered, the experimental data of which can be found in [19].

The transverse domain extends from the centerline of the jet, $y = 0$, to $y = 0.1$ m, which is approximately 12.5 times the half jet width (the half jet width is defined as a distance from the centerline of the jet to a location where the excess velocity is half the centerline excess velocity). The computational domain in the flow direction starting from $x = 0.095$ m ($x/d = 10$, $d = 0.009525$ m is the jet exit width) to $x = 0.65$ meters ($x/d = 70$) was discretized by 580 line-steps.

Decay of the centerline velocity and evolution of the half jet width along the flow direction compares favorably with experimental data as shown in Fig. 6. The computed velocity profile, turbulent kinetic energy profile, and the Reynolds stress are compared with experimental data

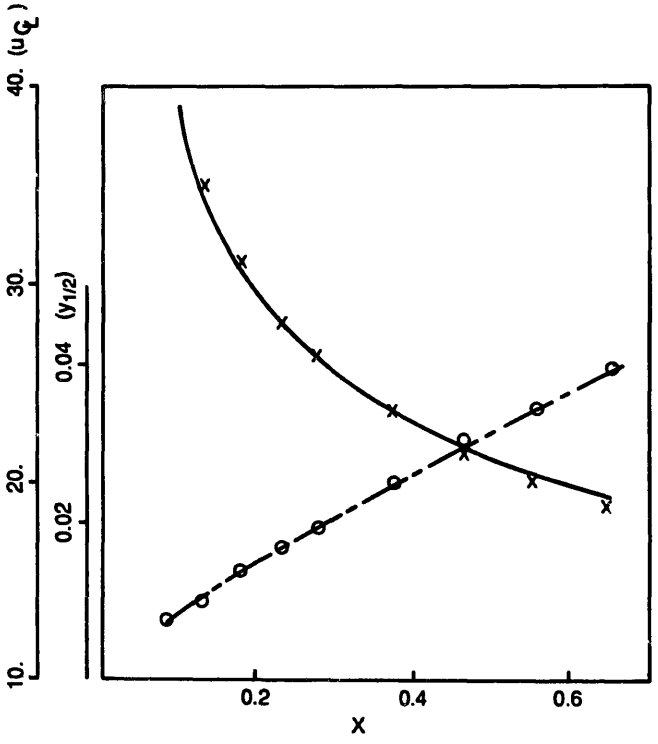

X: Exp't CENTER LINE VELOCITY, o: Exp't HALF JET WIDTH, ——: COMPUT. CENTER LINE VELOCITY, — — —: COMPUT. HALF JET WIDTH

Fig. 6. A plane jet exhausting into a moving stream.

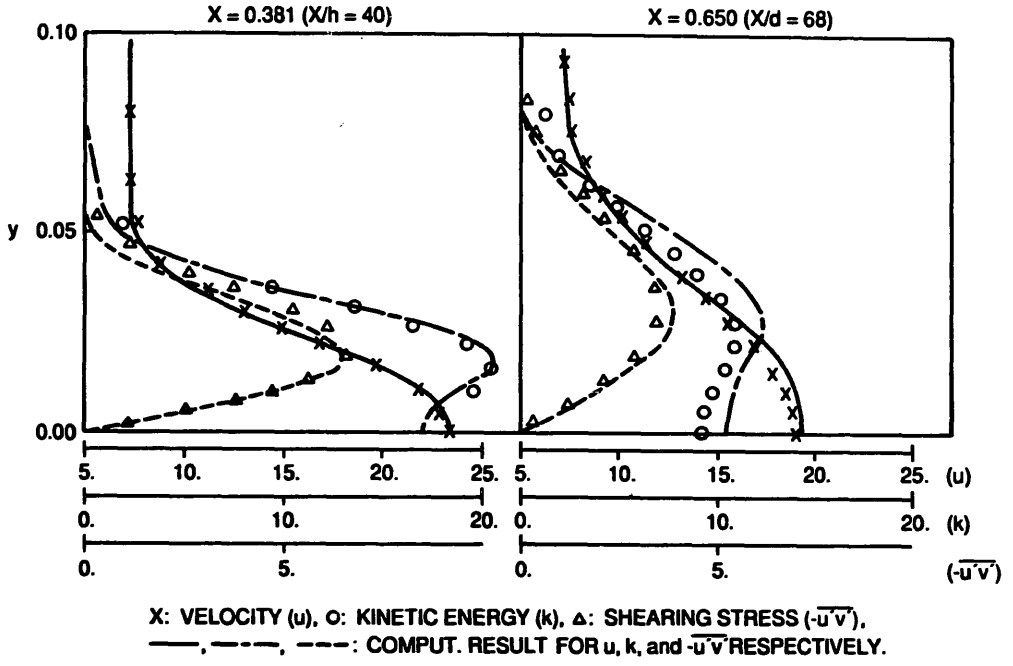

Fig. 7. A plane jet exhausting into a moving stream.

in Fig. 7 at two flow-direction locations. These profiles compare favorably with experimental data at the middle of the flow-direction domain, whereas these profiles compare less favorably with experimental data at the end of computational domain. These degenerated solutions may be due to the less appropriate c_μ function. But the global features such as the growth of the half jet width were found to be less sensitive to the c_μ function.

An average of 11 iterations was required to satisfy the convergence criterion for each line-step.

5.5. *A circular jet exhausting into a moving stream*

A circular jet experiment due to Antonia and Bilger [20] is considered herein. The turbulent kinetic energy profile for initial condition data was prepared from the experimental data of $\sqrt{(\overline{u'^2})}/u_0$, where u' is the fluctuating velocity in the flow direction and u_0 is the centerline excess velocity, by assuming that the turbulent kinetic energy would be approximately 1.2 times of the flow direction normal Reynolds stress. The computational domain in the transverse direction extends from $y = 0$ m, the centerline, to $y = 0.084$ m, which corresponds to approximately nine times the half jet width. The flow direction domain starting from $x = 0.2$ m ($x/d = 40$, where $d = 0.00528$ m is the diameter of the jet) to $x = 1.4$ m ($x/d = 265$) was discretized into 1200 line steps. An average of 6 iterations was required for each line step to achieve the convergence criterion.

Computational results showed that the flow field redeveloped due to the inaccurate turbulent kinetic energy data; and that a similarity state which is slightly different from experimental data was achieved in the far down-stream region. Decay of the centerline velocity and the growth of the half jet width are shown in Fig. 8, where it can be seen that the spreading rate at the far down-stream is close to that of the experimental data.

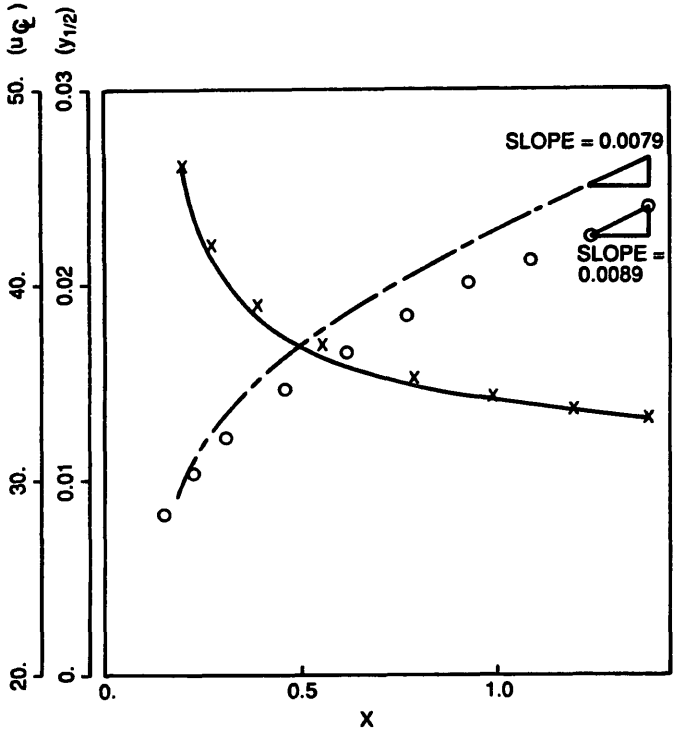

Fig. 8. A circular jet exhausting into a moving stream.

Due to the redevelopment of the flow field, the computational results are compared with experimental data in similarity coordinates, Fig. 9. It can be seen in Fig. 9 that the velocity profile is flatter than that of the experimental data in the center region of the jet, and that the gradient of velocity profile is smaller than experimental data in the middle region of the jet. The Reynolds stress profile obtained by using the Boussinesq eddy viscosity assumption that $-\overline{u'v'} = \nu_t \partial u/\partial y$ is higher than experimental data due to the smaller velocity gradient in the same middle region. These discrepancies are due to the deficiency of the c_μ function, and these degenerate computational results were not obtained in the finite difference computation of the same flow case using a constant c_μ [14].

5.6. *A wall jet issuing into a moving stream*

The wall jet is a boundary layer flow which finds a great number of applications in engineering processes. It is used in many different situations of film cooling processes and in preventing separation of boundary layer flows. The wall jet provides a serious test case for a numerical method as well as for a turbulence model, since both of these must be able to predict the behavior of wall bounded boundary layer flows and jets separately. Finite difference computation of wall jet flows can be found in [36] among many others.

One of the most complete experimental data for the wall jet flows can be found in [37]. A configuration of the wall jet is shown in Fig. 10, where b is the jet slot height, U_j is the jet exit

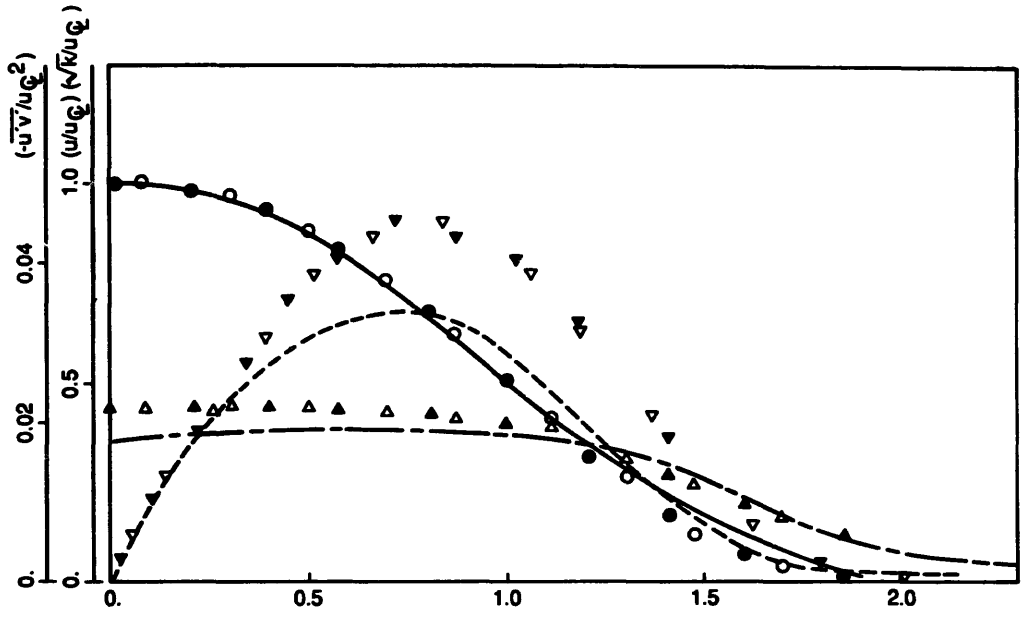

—: Exp't $\bar{u}/\bar{u}_0$; — — —: Exp't $\sqrt{\bar{u}'^2}/\bar{u}_0$; — — —: Exp't $\overline{u'v'}$; o, ● : COMPUT. u/u_0 AT X/d = 189 AND 266; △, ▲ : COMPUT $\sqrt{k}/u_0$ AT X/d = 189 AND 266; ▽, ▼ : COMPUT $-\overline{u'v'}/u_0^2$ AT X/d = 189 AND 266

Fig. 9. A circular jet exhausting into a moving stream.

velocity, $u_e(x)$ is the free stream velocity, u_0 is the maximum excess velocity, $u_m = u_0 + u_e$ is the maximum velocity, y_m is a distance from the wall to a location where $u = u_m$, and $y_{1/2}$ is the half jet width defined as the distance from the wall to the outer side location where $u = \frac{1}{2}u_0 + u_e$. Input data used in computation of the flow were obtained directly and/or by curve-fitting the experimental data [37]. These are: $b = 0.00673$ m; $U_j = 60.64$ m/s; and the

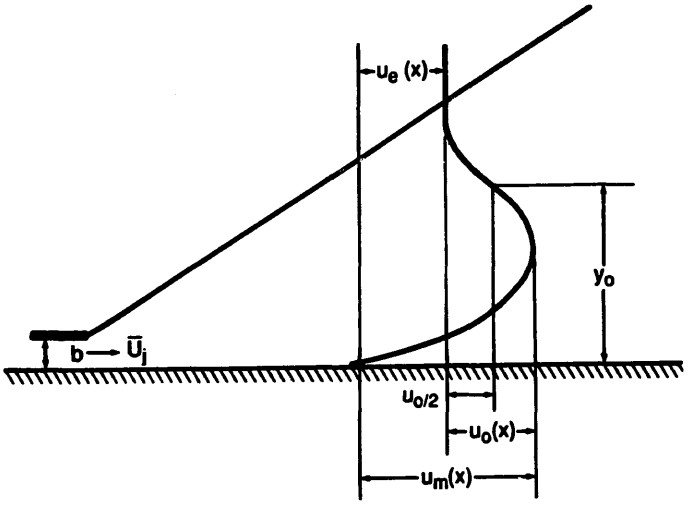

Fig. 10. Configuration of a wall jet flow.

external free stream velocity and the length-scale of the flow field are as given below:

$$u_e(x) = \frac{1}{1.65} U_j \left\{ 0.12052\left(\frac{x}{b}\right) = 0.98425 \right\}^{-0.448}, \tag{20}$$

$$\frac{y_0(x)}{b} = 0.04394\left(\frac{x}{b}\right) + 0.3819. \tag{21}$$

The computational domain extends from $y = 0.002$ m to $y = 0.08$ m in the transverse direction; and from $x = 0.5532$ m ($x/b = 82.2$) to $x = 1.6892$ m ($x/b = 251$) in the flow direction. The flow direction domain was discretized by 1135 line steps, and an average of 14 iterations was required for each line step to achieve the same convergence criterion given previously. It can be seen in Figs. 11 and 12 that computational results compares favorably with experimental data in every detail.

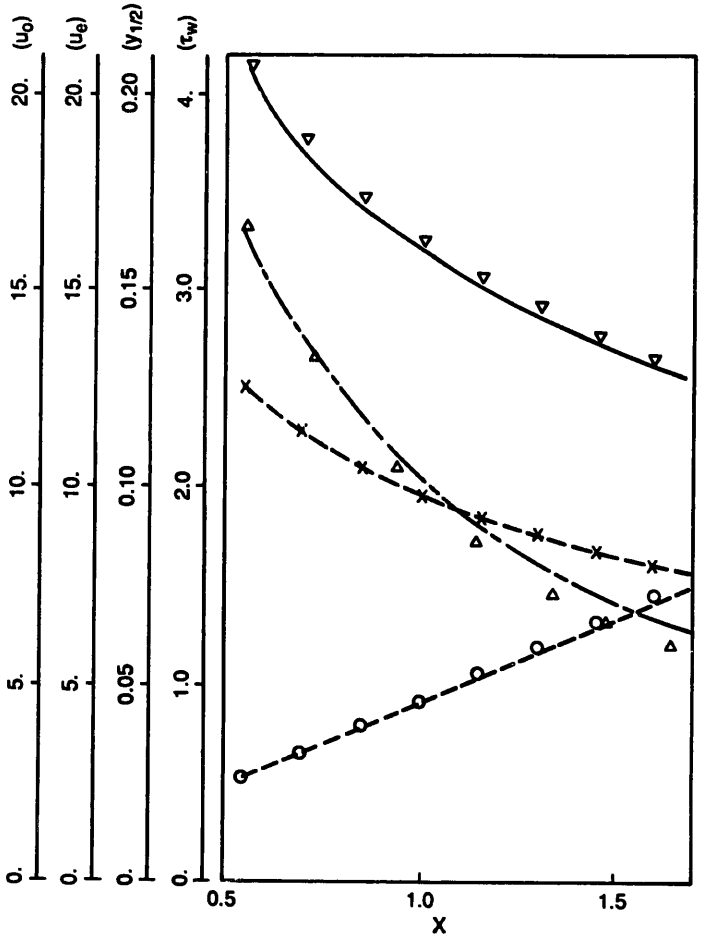

▽, X, △, O: Exp't MAX EXCESS VELOCITY (u_0), EXTERNAL VELOCITY (u_e), WALL SHEARING STRESS (τ_w), LENGTH SCALE ($y_{1/2}$) RESPECTIVELY,
——, – – –, —·—, – – –: COMPUT u_0, u_e, τ_w, $y_{1/2}$ RESPECTIVELY

Fig. 11. A wall jet flow.

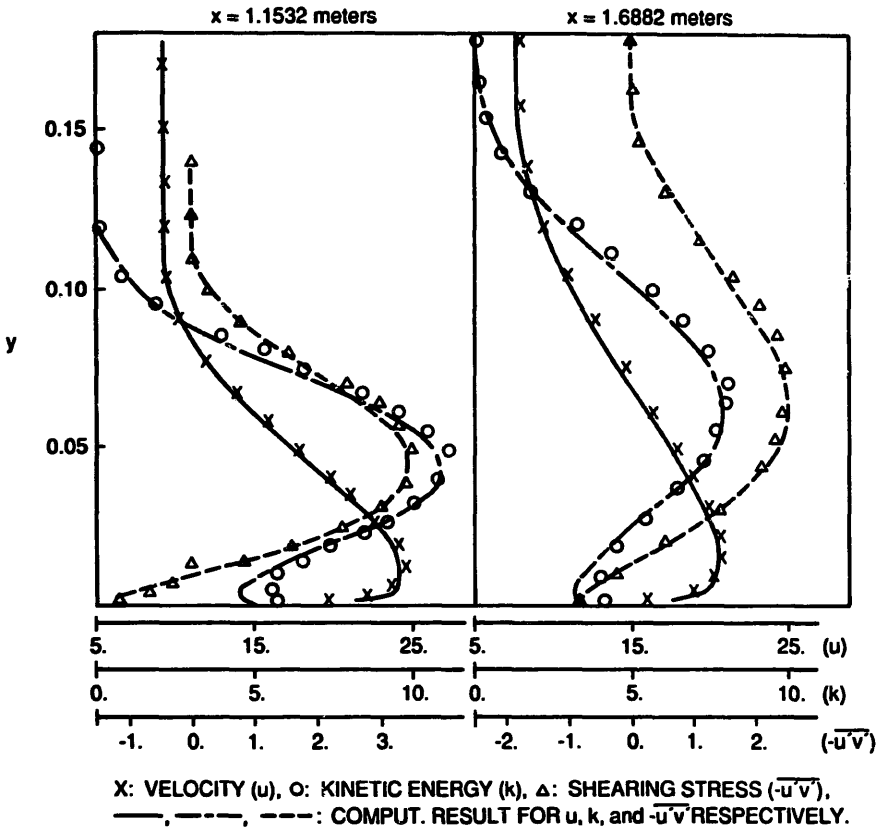

Fig. 12. A wall jet flow.

6. Conclusions

A finite element computational method for turbulent boundary layer flows and an algebraic stress turbulence model were presented. As can be found in the elliptic boundary layer flow calculations, the method yielded converged solutions using an inaccurate initial guess for all the flow variables (u, k, ε).

The newly proposed variable energy transfer function term (C_3P^2/k) has been motivated from both the physical dimensional analysis (similitude analysis) and the multiple-time-scale concept. With the use of the c_μ function which is based on experimental observations, the turbulence quantities (k and ε) seldom violated realizability in the transition region.

The successful computation of various turbulent boundary layer flows may be due to the numerical method as well as the turbulence model used. One of the accomplishment in the present study also lies in the accurate prediction of the turbulent wall jet flow without using a specifically tailored turbulence model for the flow [36].

Acknowledgment

The authors would like to express their thanks to Dr. Rand Decker (Fluid Dynamics

Branch, ED 42, NASA/MSFC) and the reviewers for their valuable suggestions in preparing the manuscript.

References

[1] D.E. Coles and E.A. Hirst, eds, Proceedings AFOSR-IFP-Stanford Conference on Computation of Turbulent Boundary Layers, Stanford, CA, 1968.
[2] S.J. Kline, B.J. Cantwell and G.M. Lilley, eds., Proceedings AFOSR-HTTM-Stanford Conference on Complex Turbulent Flows, Stanford, CA, 1981.
[3] R.M. Smith, On the finite element calculation of turbulent flow using the k-ε model, Internat. J. Numer. Meths. Fluids 4 (1984) 303–319.
[4] C. Taylor, C.E. Thomas and K. Morgan, F.E.M. and the two equation model of turbulence, in: C. Taylor and K. Morgan, eds., Computational Techniques in Transient and Turbulent Flows 2 (Pineridge Press, Swansea, U.K., 1981) 449–460.
[5] C. Taylor, T.G. Hughes and K. Morgan, Finite element solution of one-equation models of turbulent flow, J. Comput. Phys. 29 (1978) 163–172.
[6] C.E. Thomas, K. Morgan and C. Taylor, A finite element analysis of flow over a backward-facing step, Comput. & Fluids 8 (1981) 265–278.
[7] A.C. Benim and W. Zinser, Investigation into the finite element analysis of confined turbulent flows using a k-ε model of turbulence, Comput. Meths. Appl. Mech. Engrg. 51 (1985) 507–523.
[8] A.G. Hutton and R.M. Smith, On the finite element simulation of incompressible turbulent flow in general two-dimensional geometries, in: C. Taylor and B.A. Schrefler, eds., Numerical Methods in Laminar and Turbulent Flows (Pineridge, Swansea, U.K., 1981).
[9] M.O. Soliman and A.J. Baker, Accuracy and convergence of a finite element algorithm for turbulent boundary layer flow, Comput. Meths. Appl. Mech. Engrg. 28 (1981) 81–102.
[10] S.V. Patankar, Numerical Heat Transfer and Fluid Flow (McGraw-Hill, New York, 1980).
[11] M.O. Soliman and A.J. Baker, Accuracy and convergence of a finite element algorithm for laminar boundary layer flows, Comput. & Fluids (1981) 43–62.
[12] J.T. Oden and J.N. Reddy, An Introduction to the Mathematical Theory of Finite Elements (Wiley Interscience, New York, 1976).
[13] S.-W. Kim and F.R. Payne, Finite element analysis of incompressible laminar boundary layer flows, Internat. J. Numer. Meths. Fluids 5 (1985) 545–560.
[14] Y.-S. Chen and S.-W. Kim, Computation of pathological turbulent flows using an extended k-ε turbulence closure model, J. AIAA (to appear).
[15] K. Hanjalic and B.E. Launder, Contribution towards a Reynolds-stress-closure for low-Reynolds-number turbulence, J. Fluid Mech. 74 (1976) 593–610.
[16] W. Rodi, The prediction of free boundary layers by use of a two-equation model of turbulence, Ph.D. Thesis, University of London, London, 1972.
[17] B.E. Launder, A generalized algebraic stress transport hypothesis, J. AIAA 20 (1982) 436–437.
[18] P.S. Klebanoff, Characteristics of turbulence in a boundary layer with zero pressure gradient, NACA CR-1247, 1954.
[19] L.J.S. Bradbury, The structure of a self-preserving turbulent plane jet, J. Fluid Mech. 23 (1965) 31–64.
[20] R.A. Antonia and R.W. Bilger, An experimental investigation of an axisymmetric jet in a co-flowing air stream, J. Fluid Mechanics 61 (1973) 805–822.
[21] S.B. Pope, An explanation of the turbulent round-jet/plane-jet anomaly, J. AIAA 16 (1978) 279–281.
[22] K. Hanjelic and B.E. Launder, Sensitizing the dissipation equation to irrotational strains, Trans. ASME 102 (1980) 34–40.
[23] K. Hanjalic B.E. Launder and R. Schiestel, Multiple-time-scale concepts in turbulent shear flows, in: L.J.S. Bradbury, F. Durst, B.E. Launder, F.W. Schmidt and J.H. Whitelaw, eds., Turbulent Shear Flows 2 (Springer, New York, 1980) 36–49.

[24] S.-W. Kim and Y.-S. Chen, Computation of turbulent boundary layer flows with an algebraic stress turbulence model, NASA CR-178967, 1986.
[25] R.M.C. So and B.C. Hwang, Local equilibrium assumption for round jet calculation, J. AIAA 24 (8) (1986) 1388–1390.
[26] S.K. Lele, A consistency condition for Reynolds stress closure, Phys. Fluids 28 (1) (1985) 64–68.
[27] V.C. Patel, W. Rodi and G. Scheuerer, Turbulence models for near wall and low Reynolds number flows: A review, J. AIAA 23 (1985) 1308–1319.
[28] Y.-S. Chen, Application of a new wall function to turbulent flow computation, AIAA-86-0438, AIAA 24th Aerospace Sciences Meeting, Reno, NV, 1986.
[29] D.C. Wilcox, A complete model of turbulence revisited, AIAA-84-0176, AIAA 22nd Aerospace Sciences Meeting, Reno, NV, 1984.
[30] E.B. Becker, G.F. Carey and J.T. Oden, Finite Elements – An Introduction (Prentice-Hall, Englewood Cliffs, NJ, 1981).
[31] O.C. Zienkiewicz, The Finite Element Method (McGraw-Hill, New York, 3rd ed., 1977).
[32] E. Hinton, F.C. Scott and R.E. Ricketts, Local least squares stress smoothing for parabolic isoparametric elements, Internat. J. Numer. Meths. Engrg. 9 (1975) 235–256.
[33] J. Laufer, Investigation of turbulent flow in a two-dimensional channel, NACA CR-1053, 1949.
[34] J. Laufer, The structure of turbulence in fully developed pipe flow, NACA TR-1174, 1954.
[35] K. Wiehardt and W. Tillmann, Wiehardt flat plate flow, flow 1400, in: D.E. Coles and E.A. Hirst, eds., Proceedings AFOSR-IFP-Stanford Conference on Computation of Turbulent Boundary Layers, Stanford, CA, 1968.
[36] M. Ljuboja and W. Rodi, Calculation of turbulent wall jets with an algebraic stress model, Trans. ASME 102 (1980) 350–356.
[37] H.P.A.H. Irwin, Measurements in a self-preserving plane wall jet in a positive pressure gradient, J. Fluid Mech. 61 (1973) 33–63.